Chapter 10
Lipid Membrane Dynamics

Maikel C. Rheinstädter

10.1 Introduction

One of the major challenges of modern physics is how it can contribute to biology and "life sciences," which are considered as the key sciences of the twenty-first century. High-tech life sciences include the emerging biotechnology and biomedical device industries, functional foods, and nutraceuticals, and also the development of new biomaterials and pharmaceuticals. Modern physical techniques and concepts represent the most highly developed tools to access and manipulate material properties, but they are certainly underrepresented in the life sciences. Clifford Shull and Bertram Brockhouse developed elastic and inelastic neutron scattering techniques for studying structure and dynamics in condensed matter, and neutron and X-ray scattering techniques were developed and very successfully applied to investigate structure and dynamics in crystalline systems. The challenge we face is how to apply these powerful techniques to soft matter and biology, i.e., systems with a high degree of static and dynamic disorder. Even though biological membranes were studied for decades, very few biologically relevant processes were revealed on a molecular level. The reason is the combination of very small nanometer length scales and very fast dynamics of pico- and nanoseconds, which pose particular experimental challenges. The dynamics involve processes from fast motions of lipid molecules and small protein groups to slow conformational changes of large membrane areas and of membrane-embedded proteins. Neutron and X-ray scattering can be used as microscope to study structure and dynamics in these systems, because they give access to the relevant length and time scales.

M.C. Rheinstädter (✉)
Department of Physics and Astronomy, McMaster University, 1280 Main Street, West Hamilton, ON L8S 4M1, Canada and Chalk River Laboratories, Canadian Neutron Beam Centre, Chalk River ON, KOJ 1JO, Canada
e-mail: rheinstadter@mcmaster.ca

V. García Sakai et al. (eds.), *Dynamics of Soft Matter: Neutron Applications*, Neutron Scattering Applications and Techniques, DOI 10.1007/978-1-4614-0727-0_10,

Often, the structure of biomolecular systems is relatively well known and the corresponding experimental techniques, such as X-ray crystallography, nuclear magnetic resonance (NMR), and also atomic force microscopy (AFM), are well-developed standard techniques. Dynamical properties are often less well understood, but are important for many fundamental biomaterial properties such as elasticity and interaction forces. They may determine or strongly affect certain functional aspects, such as diffusion and transport through a membrane, and be relevant for protein function. Because real biological materials lack an overall crystal structure, in order to fully characterize the fluctuations and to compare experimental results with membrane theories, the measurements must cover a very large range of length and time scales [1]. The combination of various inelastic scattering techniques, such as inelastic neutron, inelastic X-ray scattering, and dynamic light scattering (DLS), enlarges the window of accessible momentum and energy transfers – or better: accessible length and time scales – and allows one to study structure and dynamics from the nearest atomic neighbor distances in lipid molecules to more than 100 nm (3 orders of magnitude), covering time scales from about one-tenth of a picosecond to almost 1 s (12 orders of magnitude). Figure 10.1 depicts the length and time scales accessible by the aforementioned techniques and more details are discussed in Chap. 1. An emerging technique is high-speed AFM which currently can deliver nanometer resolution real space images with a time resolution of milliseconds [2]. Figure 10.1 shows that combining different techniques allows us to explore the multiscale character of biological membranes [1, 3–5].

In addition and as discussed in detail in Chap. 7, Molecular Dynamics (MD) simulations are an invaluable tool to develop models for molecular structure and dynamics in membranes and proteins. Because of increasing computer power and optimized algorithms, large system sizes and long simulation times and also more and more complex systems can be addressed [7–12]. The dashed rectangle in Fig. 10.1 marks the dynamical range accessed by computer simulations. The elementary time scale in simulations is in the order of femtoseconds.

The field is currently boosted by interdisciplinary interest in life sciences. New developments and improvements in scattering instrumentation, sample preparation and environments and, eventually more powerful sources, give quantitative access to the molecular properties of bilayers on lateral length scales ranging from micrometers down to a few Angstroms (Å). Often, phospholipid bilayers are used as model systems to study fundamental properties and the structure of these systems is often well established by X-ray and neutron scattering techniques [13–19]. But the trend is to study more complex and relevant systems, decorated with cholesterol, peptides, and proteins, to eventually develop a better understanding of biological membranes.

Scattering techniques are particularly powerful in spatially ordered systems and were very successfully applied to study structure and dynamics (such as phonons) in crystals. In soft matter and biology, a periodic structure is often missing or not well developed and new concepts and approaches are required to study structural and

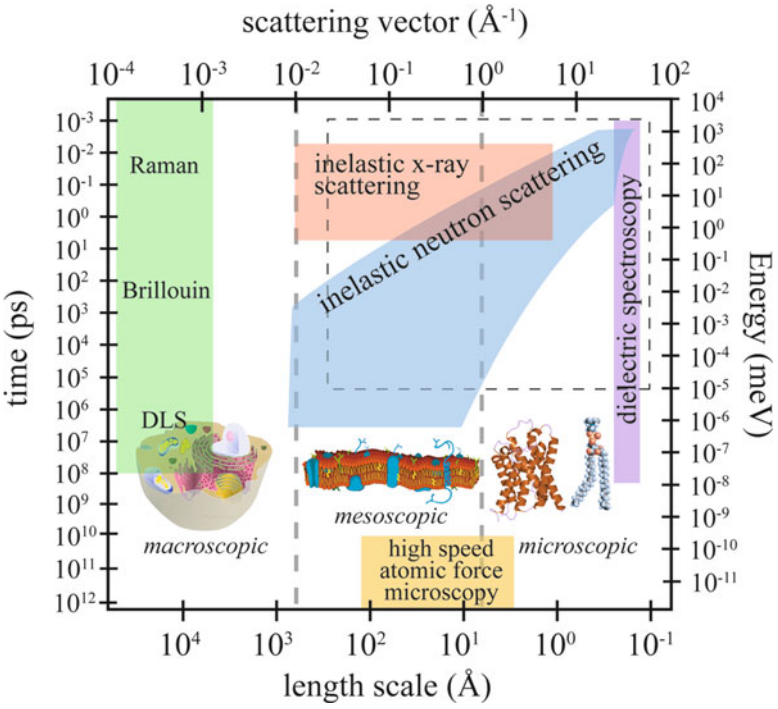

Fig. 10.1 Accessible length and time scales, and corresponding energy and momentum transfer, for some spectroscopic techniques covering microscopic to macroscopic dynamics. Light scattering techniques include Raman, Brillouin, and dynamic light scattering (DLS). Inelastic X-ray and neutron scattering access dynamics on Angstrom and nanometer length scales. Dielectric spectroscopy probes the length scale of an elementary molecular electric dipole, which can be estimated by the bond length of a C–O bond (about 140 pm). The area marked by the *dashed box* is the dynamical range accessible by computer simulations. High-speed atomic force microscopy is an emerging technique, which allows imaging in real space. For further details on some of these techniques, see Chap. 1

dynamical properties. In contrast to computer simulations where different molecular components and dynamics can be directly accessed and extracted, in experiments there is usually a superposition of signals of different molecular components and interactions, and also single-molecule and collective dynamics. By using different sample geometries, these signals can be separated by their position in reciprocal and frequency space. In particular with neutrons, selective deuteration is used to distinguish between self- and collective dynamics. In addition, because of the availability of more powerful spectrometers, smaller system dimensions and less material can be used in experiments. However, experiments are still orders of magnitude away from single-molecule spectroscopy of, for example, membrane-embedded proteins.

10.2 Structure of Membrane Systems

Membranes are disordered systems and thus it is not possible to use crystallographic measurements for a high-resolution structural characterization. The elastic X-ray and neutron scattering techniques which are mostly employed for membrane studies are small angle scattering (SAS), Small and Wide Angle Diffraction, and Specular Reflectivity. SAS is used to gain information on shape, size, and interactions of lipid lamellar systems and vesicles: it gives radial averaged information in all directions of space. SAS experiments provide information about the size, shape, and orientation of the different components of a sample for distances ranging from 50 to 5,000 Å.

Diffraction experiments are mainly used to determine the in-plane and normal structure of stacked lipid lamellar systems and can for instance locate an object within the lipid bilayer, such as a cholesterol molecule or peptides. Reflectivity is used to study the structure of bilayers in the direction perpendicular to the plane of the layers in a planar configuration and allows the determination of the structure and composition of a membrane with a very high spatial resolution. At continuous, reactor sources, collimated, monochromatic beams of wavelength λ are used to obtain a good Q and with it good spatial resolution. Spallation sources use broad wavelength bands and time of flight techniques to achieve high resolution. In both cases, the scattered beam is measured by a detector (punctual, mono, or bidimensional) and the intensity of the outgoing over that of the incoming beam recorded as a function of the wave vector transfer, Q. Scattered neutrons are not energy discriminated, but considered as scattered elastically. This assumption is usually well justified as the inelastic scattering cross-section is orders of magnitude weaker than the elastic cross-section and the intensity of inelastically scattered neutrons weak in diffraction experiments. The angle between the incoming and outgoing beams is defined as the scattering angle, 2θ. The scattering vector Q is then given by $Q = 4\pi\sin(\theta)/\lambda$. Because only the intensities of the scattered waves can be measured and not the phase shifts, a direct transformation back into real space is usually difficult.

10.3 Dynamics in Complex Membranes

Motions in proteins and biological membranes occur on various length and time scales [3, 4]. The functional behavior of membrane proteins is likely to depend on the lipid bilayer composition and physical properties, such as hydrophobic thickness and elastic moduli. Dynamics in complex membranes involve interactions between the different constituents, such as lipids, cholesterol, peptides, and proteins. How the variety of inter- and intraprotein motions, occurring over different time and length scales, interact to result in a functioning biological system remains an open field for those working at the interface of physics and biology. The dynamical coupling between proteins is thought to be important for the understanding of

macromolecular function in a cellular context because it can lead to an effective interprotein communication. The commonly assumed interaction mechanism between inclusions in membranes is a lipid-mediated interaction due to local distortions of the lipid bilayer [20–24], with a strong dependence on the bilayer properties, in particular elastic properties.

Motions in lipid bilayers range from the long wavelength undulation and bending modes of the bilayer, with typical relaxation times of nanoseconds and lateral length scales of several hundreds lipid molecules, to the short-wavelength density fluctuations in the picosecond range on nearest neighbor distances of lipid molecules [5, 6, 13, 25–31]. Local dynamics in lipid bilayers, i.e., dynamics of individual lipid molecules such as vibrations, rotations, librations (hindered rotation), and diffusion, have been investigated by, e.g., incoherent neutron scattering [25–29] and NMR [32, 33] to determine the short-wavelength translational and rotational diffusion constant.

Collective undulation modes were investigated using neutron spin-echo (NSE) spectrometers [6, 28, 29, 34] and DLS [35–37]. In contrast to other spectroscopic techniques, such as dielectric spectroscopy, inelastic X-ray and neutron scattering give a wave vector resolved access to molecular dynamics. Excitation frequencies and relaxation rates are measured at different internal length scales of the system. A typical dynamical scattering experiment measures (Q, ω) pairs, it delivers a frequency together with a corresponding length scale and possibly also corresponding direction, such as parallel or perpendicular to the protein axis. This additional information is very important to assign the measured frequencies to certain molecules or molecular components.

10.3.1 Local and Collective Molecular Motions in Membranes and Proteins

Atomic and molecular motions in membranes and proteins can be classified as local or self-correlated, and collective or pair-correlated dynamics. Local dynamics refer to the motion of molecules or functional groups in local energy potentials. The force and time constants involved are determined by the local friction and restoring forces. These types of dynamical processes are incoherent because the particles move independently in their local environments. Examples include vibrations, rotations, librations (hindered rotation), and diffusion of individual lipid molecules. In a neutron experiment, this is given by the incoherent scattering function, $S_{\mathrm{inc}}(Q, \omega)$. In contrast, the coherent scattering function $S_{\mathrm{coh}}(Q, \omega)$ gives details of the coupled, collective molecular motions which involve interactions between neighboring particles or functional groups (pictured as a spring). Coupled particles basically behave like coupled pendulums. Collective molecular motions determine, for instance, elasticity of membranes, interactions between membrane-embedded proteins, and are important for transport processes. In biology, any dynamics will most likely show a mixed behavior of particles moving in local potentials, but with a more or less pronounced coherent character.

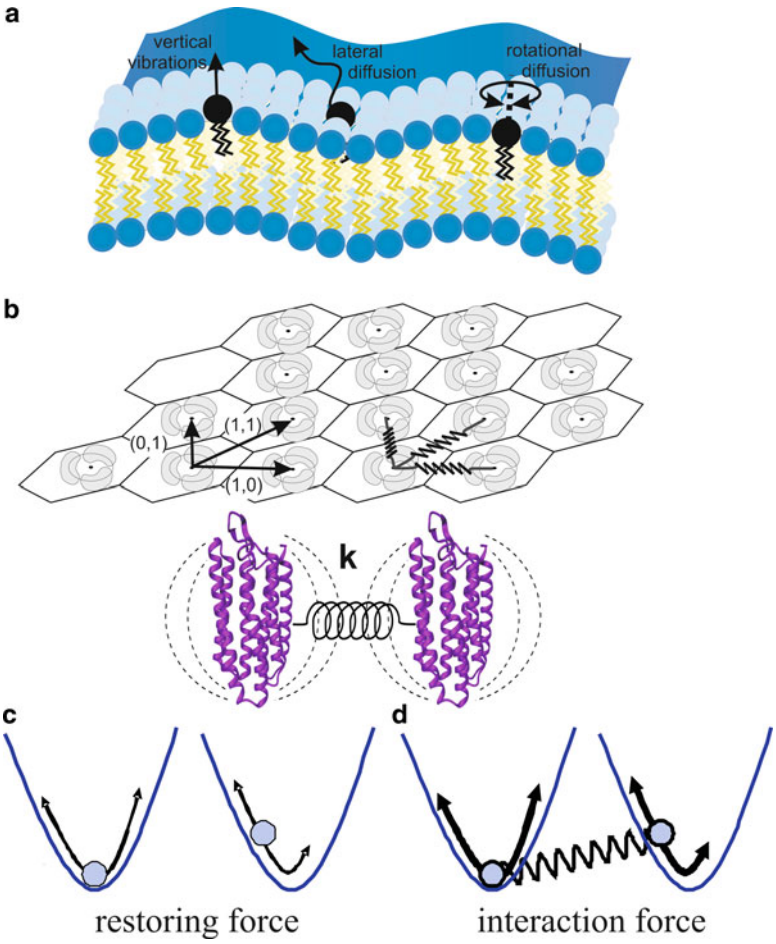

Fig. 10.2 Schematic of some elementary dynamical modes occurring in lipid bilayers. (**a**) Local modes include diffusion and vibrations, rotations, and librations (hindered rotations) of single lipid molecules, (**b**) coupling of membrane-embedded proteins in a hexagonal arrangement, taking bacteriorhodopsin in purple membrane as an example. The interaction between protein trimers is depicted as springs with effective spring constant k, (**c**) motion of molecules or functional groups in local energy potentials, which gives rise to incoherent dynamics, and (**d**) interaction between particles as probed via coherent dynamics measurements

Figure 10.2 depicts some of the local and collective modes occurring in a phospholipid bilayer. Rotational and lateral diffusion, vibrations, and rotations of the single lipid molecules can be investigated by, e.g., incoherent inelastic neutron scattering, NMR, or dielectric spectroscopy (Fig. 10.2a, c). Only coherent probes, such as coherent inelastic neutron scattering or inelastic X-ray scattering, can elucidate collective molecular motions, depicted as a system of coupled membrane-embedded proteins in Fig. 10.2b, d.

Table 10.1 Coherent and incoherent scattering lengths and cross-sections for selected elements as provided by the NIST Center for Neutron Research (http://www.ncnr.nist.gov/resources/n-lengths/)

Nuclide	b_{coh} (fm)	b_{inc} (fm)	σ_{coh} (b)	σ_{inc} (b)
^{1}H	−3.7406	25.274	1.7583	80.27
^{2}H	6.671	4.04	5.592	2.05
^{3}H	4.792	−1.04	2.89	0.14
^{14}N	9.37	2.0	11.03	0.5
^{15}N	6.44	−0.02	5.21	0.00005
^{12}C	6.6511	0	5.559	0
^{13}C	6.19	−0.52	4.81	0.034
^{16}O	5.803	0	4.232	0
^{17}O	5.78	0.18	4.2	0.004
^{18}O	5.84	0	4.29	0

Note that 1 b = 1barn = 10^{-28} m^2 = 100 fm^2

10.3.2 Selective Deuteration and Labeling Techniques

In neutron scattering, the total scattering of a sample will consist of coherent and incoherent scattering contributions. The fraction of coherent and incoherent scattering depends on the atomic composition and the respective scattering lengths. Substitution of certain elements in a compound by their isotopes may increase contributions of certain molecules or functional groups to the coherent or incoherent scattering contribution.

The coherent and incoherent neutron cross-sections, b_{coh} and b_{inc}, of an element can be illustrated by two extreme cases. If all the nuclei in a sample have different b's, there is no interference between the different atoms. The incoherent scattering therefore depends only on the correlation between the positions of the same nucleus at different times. Incoherent scattering therefore probes the local atomic or molecular environment. If all scattering lengths are the same, i.e., all nuclei are identical for the neutron probe, the coherent scattering still depends on the correlation between the positions of the same nucleus at different times, but also on the correlation between the positions of different nuclei at different times. It therefore gives interference effects and allows to measure interaction forces. In general, every element has coherent and incoherent scattering lengths. Table 10.1 lists the scattering lengths for selected elements, which are common in biological materials.

Most noticeable are the very large incoherent cross-section for hydrogen, ^{1}H, and the relatively large coherent cross-section for deuterium, ^{2}H. This is important for selective deuteration, as will be discussed below. The incoherent cross-section of hydrogen atoms is about 40 times larger than that of deuterium and of all other atoms present in biological macromolecules. Consequently, hydrogen atoms dominate the incoherent scattering signal of biological samples. The hydrogen atoms reflect the movements of larger groups to which they are attached, such as amino acid side chains. Deuteration, i.e., the substitution of protons by deuterium (^{2}H), is often

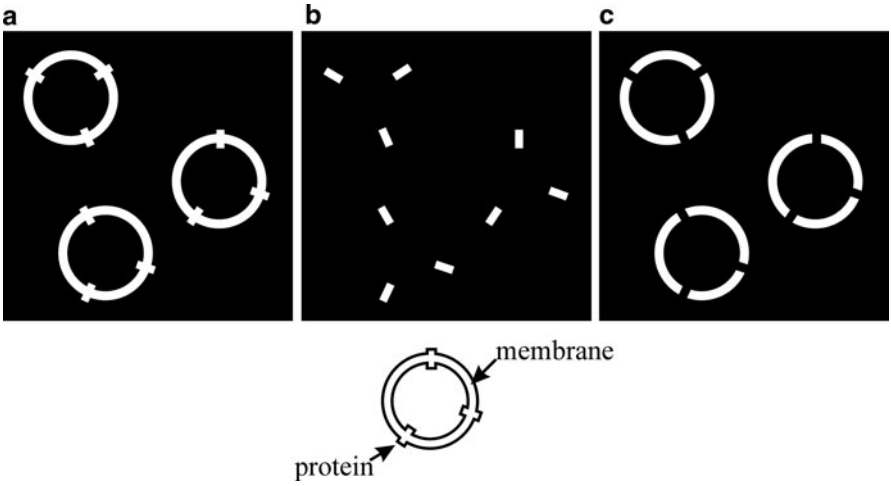

Fig. 10.3 Schematic example of how selective deuteration can be used to highlight molecules or functional groups in neutron scattering experiments. Depicted are lipid vesicles (*ring*) with embedded proteins (shows are *rectangles*) in a solvent: (**a**) hydrogenated membrane and embedded proteins in a deuterated solvent, thus visible in incoherent neutron scattering experiments, (**b**) solvent and membrane are deuterated, allowing the investigation of the local dynamics of the embedded proteins, and (**c**) deuterated proteins and solvent allow investigating membrane dynamics

used to suppress the incoherent scattering contribution of certain functional groups to the total scattering. While in protonated samples the incoherent scattering is usually dominant and the time self-correlation function of individual scatterers is accessible, (partial) deuteration emphasizes the coherent scattering and gives access to collective motions by probing the pair correlation function.

We try to explain this with the example of a protein embedded in a lipid membrane dissolved in a common solvent. This is shown schematically in Fig. 10.3. In a sample where both the membrane and the proteins are hydrogenated but the solvent is deuterated, self-correlated, diffusive motions of membranes and embedded proteins are probed (Fig. 10.3a). Diffusive dynamics of the proteins are highlighted when solvent and membrane are deuterated, and hydrogenated proteins are used (Fig. 10.3b). The effect of protein insertion on membrane dynamics can be studied in Fig. 10.3c, with deuterated solvent and proteins. Note that at the same time, the interfaces between protonated and deuterated areas scatter coherently. The preparation in Fig. 10.3c can therefore be used to study possible protein–protein interactions.

A typical neutron spectrum, measured by inelastic X-ray or neutron scattering at a particular Q-vector, is shown in Fig. 10.4. The total signal typically consists of a sharp peak at energy transfer zero, which marks the instrumental resolution. The resolution is often well described by a Gaussian peak shape. Quasielastic scattering is observed as a broadening of the instrumental resolution. In addition, inelastic

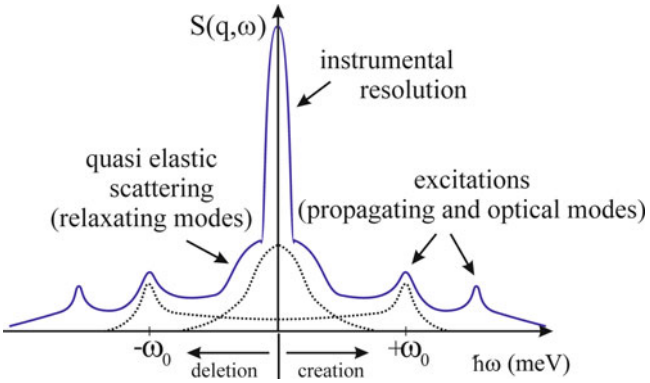

Fig. 10.4 Typical excitation spectrum for X-rays and neutrons. The signal consists of a *sharp central line*, the instrumental resolution, a broad component centered at energy transfer zero (quasielastic scattering), and pairs of excitations

peaks may be observed. Excitations always occur as pairs of inelastic peaks at frequencies of $-\omega_0$ and $+\omega_0$, caused by creation and deletion of dynamical modes. Starting from the simple models for local and collective modes in Fig. 10.2c, d, assumptions for peak shapes of the corresponding modes can be developed. Typical local modes, such as diffusion and libration (hindered rotation), are examples for relaxators, i.e., overdamped oscillations. The characteristic frequency of a relaxator is $\omega_0 = 0$, so that the response is centered on the elastic line. The width of the response is determined by the relaxation time τ_0, $\Delta\hbar\omega = 2\pi/\tau_0$. In the time domain, a relaxation is described by an exponential decay e^{-t/τ_0}, the Fourier transform of which is a Lorentzian function. So local, incoherent dynamics give rise to a quasielastic broadening in the energy domain and are described by Lorentzian line shapes, centered at energy transfer zero. Coherent dynamics probe the elastic springs between molecules or atoms. They can be considered as particles bound by an isotropic harmonic force and damped through hybridization with a phonon bath. Those propagating (acoustic) or oscillating (optical) modes have well-defined eigenfrequencies and lead to inelastic excitations at energy values $\pm\hbar\omega_0$. They are described by a damped harmonic-oscillator model. The width of the inelastic peak is related to the lifetime of the excitation. A strict derivation of the peak profiles can be found in the books by Squires [38] and Lovesey [39].

The origin of quasielastic and inelastic scattering is purely coherent for X-rays. In the case of liquids, for instance, the spectrum can be evaluated by a generalized effective eigenmode theory [40] in terms of a heat mode (a collective diffusion process) and sound modes. For neutrons, the quasielastic part of the spectrum can have contributions from coherent and incoherent scattering, but is most likely dominated by the incoherent scattering of hydrogen atoms. The corresponding dynamical modes are relaxating local modes, such as diffusion of molecules or functional groups. The relaxation times can be determined from the width of

a Lorentzian peak shape. Excitations stem from coherent scattering and involve dynamics between different particles from interference effects. So by preparing a hydrogenated or deuterated sample and tuning the spectrometer to quasi- or inelastic scattering (QENS or INS respectively), a neutron scattering experiment can be made sensitive to local or collective dynamics.

Collective molecular motions impact on, e.g., properties and functionalities of artificial and biological membranes, such as elasticity, transport processes, and determine interaction between proteins. Two examples will be discussed in detail in what follows with emphasis on the dynamics-property and dynamics-function aspects of the experiments:

1. Mesoscopic shape fluctuations in aligned multilamellar stacks of 1,2-dimyristoyl-*sn*-glycero-3-phoshatidylcholine (DMPC) bilayers were studied using the NSE technique. From the dispersion relation in the fluid phase, values for the bilayer-bending rigidity κ, the compressional modulus of the stacks B, and the effective sliding viscosity η_3 were determined (Sect. 10.4.2). This technique offers a novel approach to quantify the elasticity parameters in membranes by direct measurement of dynamical properties and also the impact of collective molecular motions on membrane properties [6].
2. Experimental evidence for a protein-protein interaction between the bacteriorhodopsin proteins in purple membrane (PM) was found by inelastic neutron scattering (Sect. 10.4.3). The dynamics were quantified by measuring the spectrum of the acoustic phonons in the two-dimensional (2D) Bacteriorhodopsin (BR) protein lattice. In this case, INS was used to study interactions between constituents of a biological membrane [68].

10.3.3 Techniques in Brief: Inelastic Neutron Scattering Instruments

Only recently, the first inelastic scattering experiments in phospholipid bilayers to determine collective motions of the lipid acyl chains were performed using inelastic X-ray [41] and neutron [42] scattering techniques. In the case of single membranes, the scattering signal is usually not sufficient for a quantitative study of the inelastic scattering. To maximize the scattering signal, multilamellar samples composed of stacks of several thousands of lipid bilayers separated by layers of water are necessary. A high orientational order of the samples which gives rise to pronounced Bragg peaks and excitations is a prerequisite to a proper analysis of the corresponding correlation functions. The use of well-oriented samples leads to well-localized elastic and inelastic signals in reciprocal space and allows distinguishing motions in both the plane of the membrane $(q_{||})$ and perpendicular to the bilayers (q_z). During the experiments, the membranes were kept in a humidity chamber to control temperature and humidity and were hydrated with D_2O from the vapor

phase. The collective motions of the lipid acyl chains were probed by using partially, chain-deuterated lipids (DMPC-d54). The experiments discussed here were conducted on two different types of neutron spectrometers, namely triple-axis and spin-echo spectrometers. Technical details and accessible length and time scales of the spectrometers are discussed in more detail in [6,43]. Here only a brief description of the techniques is given.

NSE spectrometry. Fluctuations on the mesoscopic scale are determined by the elasticity parameters of the bilayers, i.e., the compressibility of the stacked membranes, B, and the bending modulus κ. The relaxations in this regime are in the nanosecond time-range with accompanying small Q-vales. NSE spectrometers are highly suited for these experiments. The NSE technique offers extremely high-energy resolution from Larmor tagging the neutrons: the neutron's spin is used as an individual label to measure the velocity and energy of the neutron by counting the number of Larmor precessions in a well-defined magnetic field. A neutron spin-echo measurement is in essence a measurement of neutron polarization [43]. The polarized neutron beam passes through a magnetic field perpendicular to the neutron polarization and neutron spin precesses before arriving at the sample, acquiring a precession angle φ_1. At the sample, the beam is scattered before passing through a second arm, acquiring an additional precession angle φ_2 in the reversed sense. For elastic scattering, when the velocity in the two arms is identical, the total precession angle is $\Delta\varphi = \varphi_1 - \varphi_2 = 0$ for all incoming neutron velocities. If the neutron scatters inelastically by gaining or losing a small energy transfer $\hbar\omega$ (the velocity v_2 in the second arm is faster or slower than v_1), there will be a linear change $\Delta\varphi = \tau\omega$ with τ being a real time in the case of quasielastic scattering. The spin-echo technique thus works in the time domain and measures the intermediate scattering function $S(Q, t)$ in contrast to the three-axis technique. For a quasielastic response, assumed to have Lorentzian lineshape with half-width Γ, the polarization will then show a single exponential decay $P_{\mathrm{NSE}} = P_{\mathrm{s}}\mathrm{e}^{-\Gamma t}$.

Triple-axis spectrometry. Fast motions in the picosecond time-range due to sound propagation in the plane of the bilayer are best measured on triple-axis spectrometers. The energy of the incident and scattered neutrons is determined by Bragg scattering from crystal monochromators (graphite in most cases). Advantages of triple-axis spectrometers are their relatively simple design and operation and the efficient use of the incoming neutron flux to the examination of particular points in (Q, ω) space. By varying the three axes of the instrument, the axes of rotation of the monochromator, the sample, and the analyzer (as depicted in Fig. 10.5a), the wave vectors k_{i} and k_{f} and the energies E_{i} and E_{f} of the incident and the scattered neutrons, respectively, can be determined. The momentum transfer to the sample and the energy transfer, $\hbar\omega$, are then defined by the laws of momentum and energy conservation to $Q = k_{\mathrm{f}} - k_{\mathrm{i}}$ and $\hbar\omega = E_{\mathrm{i}} - E_{\mathrm{f}}$. The accessible (Q, ω) range is limited by the range of incident neutron energies offered by the neutron guide, as well as by mechanical restrictions of the spectrometer.

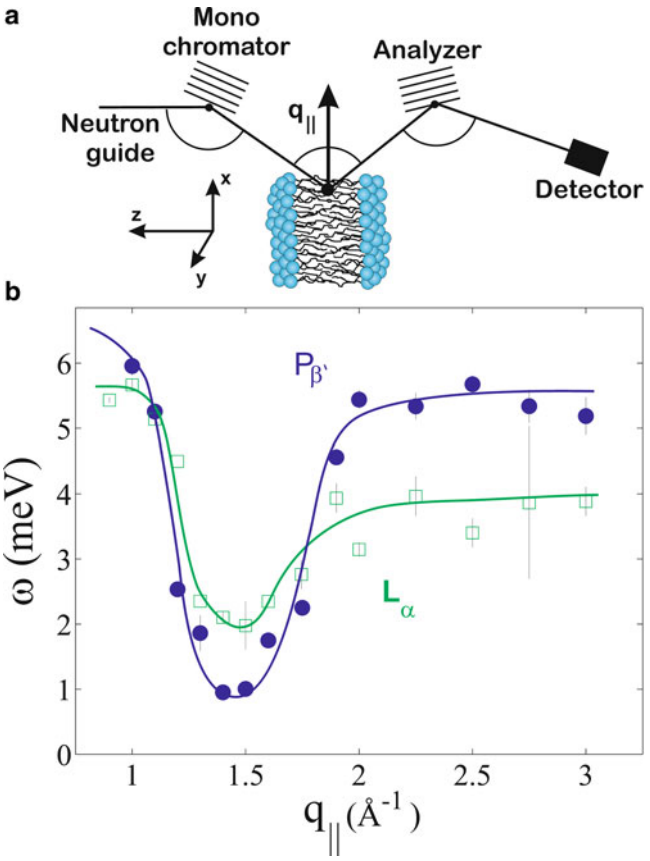

Fig. 10.5 (**a**) Schematic of a triple-axis spectrometer. (**b**) Short-wavelength dispersion relations in the gel ($P_{\beta'}$) and fluid phase L_α of the phospholipid (DMPC) bilayers [42]

10.4 Collective Molecular Dynamics in Membranes and Proteins

10.4.1 Dispersion Relations

Collective molecular motions in membranes and proteins are attracting increasing attention as they are speculated to be responsible for certain functionalities in model membranes, such as transport of small molecules, pore opening, and membrane fusion processes. Collective motions of functional groups may drive protein function. In a cellular context, they may contribute to the understanding of macromolecular function because they can lead to an effective coupling and communication between the different constituents.

Collective motions can be modeled by interacting particles, as sketched in Fig. 10.2b, d. The corresponding dynamics is described by a set of coupled pendulums (particles bound by an isotropic harmonic force). In inelastic scattering experiments, excitation energies are probed at different internal length scales and different directions. The Q-dependence of the excitation energies is usually not a trivial function. The energies will depend on the interaction constant, k, but also on the geometrical arrangement of the objects. It will depend on the length scale, the Q-value, but critically also on the coupling path, i.e., the direction, which is probed, as depicted in Fig. 10.2b. A typical experiment to measure collective dynamics records excitation frequencies at different Q-values (different internal length scales) over a continuous Q-range. The corresponding curve $\hbar\omega(Q)$ is called a dispersion relation. It describes the complex dynamics of a (oriented) system of coupled oscillators. Technically, it describes the way waves with a certain wavelength propagate through the system. Only coherent probes are capable to elucidate coherent dynamics.

Chain-deuterated lipids (DMPC-d54) hydrated by heavy water (D_2O) were used to enhance the contribution of the collective motions of the lipid acyl chains over other contributions to the total scattering. The samples were kept in a closed temperature and humidity-controlled aluminum chamber. Hydration of the lipid membranes was achieved by separately adjusting two heating baths, connected to the sample chamber and to a heavy water reservoir, hydrating the sample from the vapor phase. Temperature and humidity sensors were installed close to the sample. d-spacings of 53 Å were achieved. The corresponding relative humidity (RH) can be determined from d-RH curves (for instance from Figure 3 in ref. [44]) to be 99.5%. The main transition in DMPC occurs at 23.4 °C [45]. The transition temperature, T_m, is slightly lowered in the deuterated compound (DMPC-d54) to about 21°C [46].

Figure 10.5b shows the short-wavelength dispersion relation in a DMPC membrane. The experiments were performed using the IN12 cold triple-axis spectrometer at the Institut Laue Langevin (ILL), Grenoble, France. The particular shape of the corresponding dispersion relation can qualitatively be explained as follows: at small $q_{||}$, longitudinal sound waves in the plane of the bilayer are probed and give rise to a linear increase of $\omega \sim q_{||}$. The low q-range of the dispersion is difficult to access by inelastic neutron scattering because of the kinematic restriction. Because of the distinct particle character of neutrons, the corresponding dispersion relation is proportional to $\hbar^2/2m_n q^2$ (with neutron mass m_n). The parabolic shape of the neutron dispersion prevents inelastic experiments at small q-values and at the same time high-energy transfers. This is called the kinematic restriction.

The lipid dispersion saturates at some maximum value, before a pronounced minimum is observed at $q_0 \approx 1.4\,\text{Å}^{-1}$, the average nearest neighbor distance of two lipid chains of $2\pi/1.4\,\text{Å}^{-1} \approx 4.5\,\text{Å}$. q_0 can be interpreted as the center of the first Brillouin zone of a two-dimensional liquid. Collective modes with a wavelength of the average nearest neighbor distance $2\pi/q_0$ are energetically favorable leading to a minimum in the dispersion relation. In highly ordered crystalline systems, the energy of the longitudinal phonon branches goes to zero at the zone centers. Here, the high degree of static and dynamic disorder in the lipid bilayers eventually

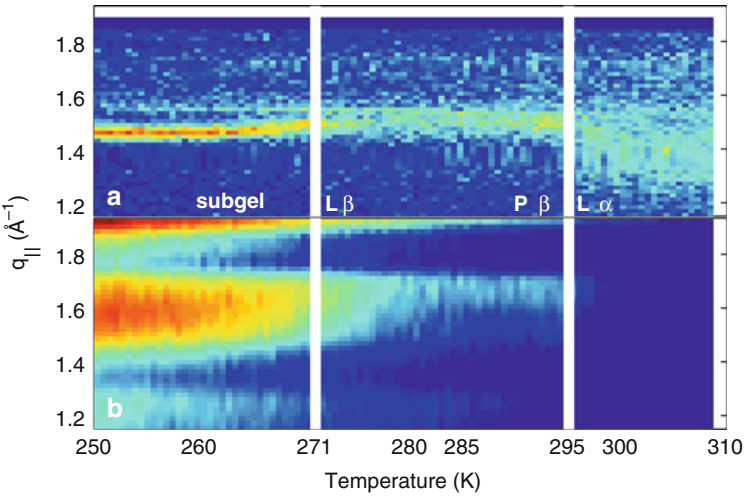

Fig. 10.6 Chain correlation peak in DMPC as measured with (**a**) energy-integrated neutron diffraction for temperatures $250 < T < 310$ K to cover gel, ripple, and fluid phase. (**b**) "True" elastic scattering, measured with an energy resolution of 0.9 μeV using a neutron backscattering spectrometer (from ref. [47]). No elastic intensity is observed in the fluid phase of the lipid bilayer

leads to a minimum at finite energy values (soft-mode). Two comments are in order: q_0 is usually the position of the first maximum in the static structure factor $S(q_{||})$ measured in neutron and X-ray diffraction experiments. When measuring diffraction, the energy of the scattered neutrons or X-rays is not discriminated. However, in a study of in-plane diffraction using a high-energy resolution of 0.9 μeV (corresponding to a timescale of about 1 ns) backscattering spectrometer [47], there was no truly elastic intensity observed in the fluid phase of a DMPC bilayer, as shown in Fig. 10.6. The structures usually observed in diffraction experiments in fluid phases of lipid bilayers are therefore dynamic with lifetimes in the order of nanoseconds, only. Secondly, the in-plane structure of lipid bilayers is often characterized in experiments by the position of the average nearest neighbor lipid tail correlation peak. However, the parameter used in molecular dynamics simulations is usually the area per lipid, rather than the nearest neighbor distance. The determination of exact areas per lipid from experiments is a very active field of research and important to compare experiments and simulations. While it is not possible to relate the area per lipid straightforwardly to the inter chain distance [48], precise lipid areas could be determined by combining neutron and X-ray scattering techniques [49].

A quantitative theory which predicts the absolute energy values of maximum and minimum on the basis of molecular parameters is absent so far. However, the dispersion relation can be extracted from molecular dynamics simulations by temporal and spatial Fourier transformation of the molecular real space coordinates [9] which shows excellent agreement with the data. Note that the dispersion relation

found is similar to those in ideal liquids, e.g., liquid argon [50,51], liquid neon [52], or liquid helium [53]. The interior of the lipid bilayer, the C-atoms or C–D groups of the lipid acyl chains, behave like a quasi liquid. In contrast to real liquids, the chain atoms of the lipid molecules are chemically bound to each other, leading to smaller mobility and diffusion and, as a consequence, pronounced excitations.

To establish possible dynamics-function relations, such as a connection with transmembrane transport, the dispersion relation in a membrane-containing drug enhancers will be studied. It is speculated that the soft-mode in such a system drop down to small energy values because enhanced fluctuations of the lipid chains may be the driving transport mechanism.

10.4.2 Membrane Properties

According to linear smectic elasticity theory [54, 55], thermal fluctuations in the fluid phase of the membrane are governed by the free energy functional (Hamiltonian):

$$H = \int_A \mathrm{d}^2 r \sum_{n=1}^{N-1} \left(\frac{1}{2} \frac{B}{d} (u_{n+1} - u_n)^2 + \frac{1}{2} \kappa \left(\nabla_{||}^2 u_n \right)^2 \right), \tag{10.1}$$

where κ denotes the bilayer-bending rigidity, A the area in the xy-plane, N the number of bilayers, and u_n the deviation from the average position nd of the nth bilayer, d is the lamellar spacing. B and $K = \kappa/d$ are elastic coefficients, governing the compressional and bending modes of the smectic phase, respectively. A fundamental length scale in these systems is given by the smectic penetration length $\Lambda = \sqrt{K/B}$. Aligned lipid bilayers allow a separate determination of both parameters K and B [56,57].

Figure 10.7 shows the intermediate scattering function $S(q_{||},t)$ for selected $q_{||}$ values. The experiments were performed on the spin-echo spectrometers IN11 and IN15 at the ILL. Data have been taken at three different temperatures, at 19 °C, in the gel (ripple, $P_{\beta'}$) phase of the phospholipid bilayers, at 22 °C, just above the temperature of the main transition, and at 30 °C, in the fluid L_α phase of the membranes and above the regime of the so-called anomalous swelling. Two relaxation processes, one at about 10 ns (τ_1) and a second, slower process at about 100 ns (τ_2), were observed. The relaxation rates ${\tau_1}^{-1}$ and ${\tau_2}^{-1}$ in the gel and the fluid phase are shown in Fig. 10.7a, b. Both relaxation branches are dispersive. The fast process shows a ${q_{||}}^2$ increase at small $q_{||}$ values and a bend at about $q_{||} \sim 0.015\,\text{Å}^{-1}$. The dispersion in the gel phase and close to the phase transition in Fig. 10.7b appears to be more pronounced as compared to the fluid 30 °C dispersion. A soft-mode appeared in the $T = 22$ °C dispersion, indicating a significant softening of the bilayer at a well-defined wave number. The slow branches at $T = 19$ and 30 °C also show increasing relaxation rates with increasing $q_{||}$ values, but with a distinct nonpolynomial behavior.

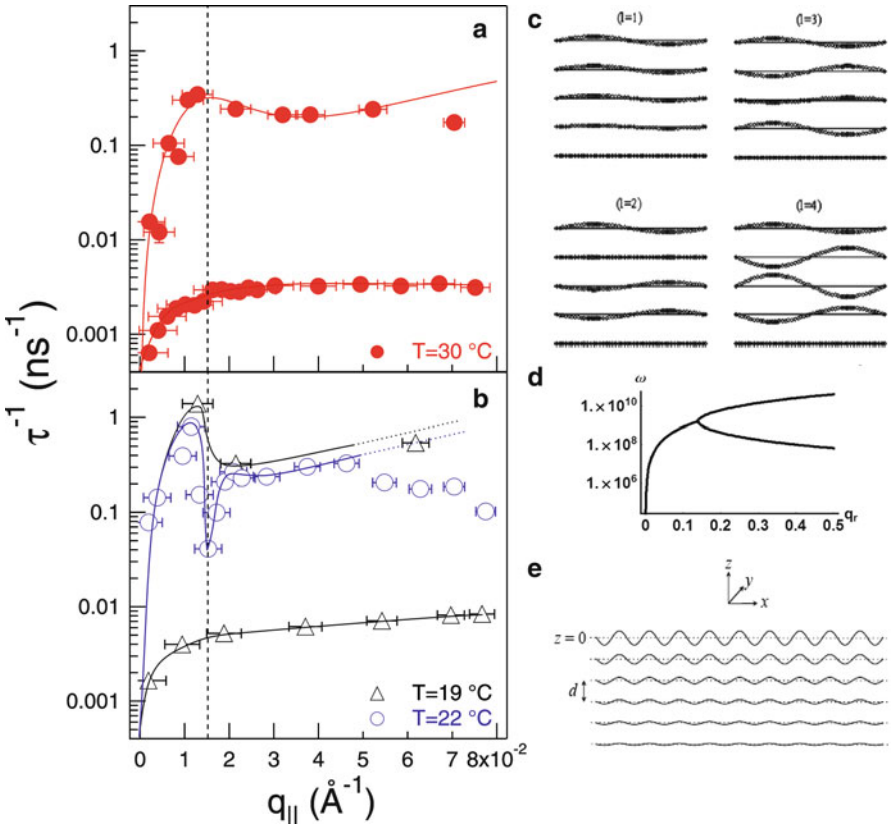

Fig. 10.7 (**a**) Dispersion relations in the fluid phase of the phospholipid bilayers, at $T = 30\,^{\circ}\mathrm{C}$. The *solid line* is a fit to Equation (10.2) [6]. (**b**) Dispersion relations in the gel $(19\,^{\circ}\mathrm{C})$ and in the range of critical swelling $(22\,^{\circ}\mathrm{C})$. A pronounced soft-mode is observed at $q_0 = 0.015\,\mathrm{Å}^{-1}$ at $22\,^{\circ}\mathrm{C}$ marked by the *dotted vertical line*. (**c**) Fluctuation spectrum of solid-supported multilamellar membranes [58], and corresponding analytical dispersion relation (**d**). (**e**) Surface mode which is responsible for the slow relaxation branch in part (**a**) [59, 60]

The dispersion relation of the fast branch with relaxation rates between 1 and 10 ns can be attributed to undulation dynamics. Qualitatively, at very small $q_{||}$-values, the membranes behave as liquid films and their dynamics are basically determined by the viscosity of the water layer in between the stacked membranes (film regime). With increasing $q_{||}$, there is a transition into a bulk-elasticity regime where the dynamics depend on the elastic properties of the lipid bilayers. At this point, the dispersion bifurcates in two relaxation branches. The faster one, which is out the experimentally accessible time window of the NSE spectrometer, is mainly determined by the compressional module B. The fluctuation spectrum of solid-supported membranes was modeled analytically [58] and is depicted in Fig. 10.7c. Quasiacoustic and optical modes were found (quasi because the modes are not

propagating due to the solid support) with increasing fluctuation amplitudes towards the center of the membrane stack. The calculated dispersion of the quasiacoustic branch is shown in Fig. 10.7d, and the shape qualitatively agrees well with the measured data. The slower branch, which is observed here, can be assigned to the bending modulus κ. The additional slow dispersion branches in Fig. 10.7a, b with relaxation rates of about 100 ns could be attributed to a surface relaxation mode [59, 60]. The mode is depicted in Fig. 10.7e and particular to a stack of membranes.

Following the idea of Ribotta et al. [61], the relaxation rates of the undulations can be described by:

$$\tau^{-1}(q_{||}) = \frac{\kappa/d}{\eta_3} q_{||}^2 \frac{q_{||}^4 + (\pi/\Lambda D)^2}{q_{||}^4 + (\pi/D)^2/\mu\eta_3}, \tag{10.2}$$

(where η_3 is the layer sliding viscosity), and the following results were obtained: $\kappa = 14.8 k_B T$, $\Lambda = 10.3\,\text{Å}$, $\eta_3 = 0.016\,\text{Pa s}$. B was calculated to be $B = 1.08 \times 10^7\,\text{J/m}^3$ ($d = 54\,\text{Å}$). The resulting effective sliding viscosity of the membrane system η_3 was found to be 16 times higher than that of water, what points to different properties of the interstitial hydration water, as compared to bulk water. Equation (10.2) does not describe a pure undulation mode, which is probed at q_z values of $q_z = 2\pi/d$, only. If the scattering is probed at finite components $\Delta q_z := (q_z - 2\pi/d)$ or measured with a relaxed q_z resolution, there is a mixing of baroclinic modes, which are distinctly slower than a pure undulation because they involve a relocation motion of the water layer. The parameter D describes an effective finite-size cutoff-length, which was related to the instrumental resolution $D = \pi/\Delta q_z$.

From the soft-mode in the fluid dispersion at $T = 22\,^\circ\text{C}$, it can be concluded that the well-known softening of phospholipid membrane upon approaching the main phase transition temperature from the fluid phase, i.e., the regime of critical swelling or anomalous swelling [44], occurs on a well-defined length scale, only $(2\pi/q_{||} \sim 420\,\text{Å})$. The elastic parameters of membranes can also be determined by analysis of the diffuse nonspecular scattering. The most important contribution of inelastic measurements and the determination of a dispersion relation is that the stiffness of the bilayers is determined as a function of internal length scale.

10.4.3 Interactions in Membranes

Recently, interprotein motions in a carboxymyoglobin protein crystal were reported from a molecular dynamics simulation [12, 72]. Experimentally, phonon-like excitations of proteins in hydrated protein powder were reported [73]. Finally, Protein–protein interactions in a biological membrane, the purple membrane (PM), were reported from inelastic neutron scattering [68].

PM occurs naturally in the form of a two-dimensional almost crystal-like structure, consisting of 75% (wt./wt.) of a single protein, bacteriorhodopsin (BR), that functions as a light-activated proton pump, and 25% various lipid species (mostly phospho- and glyco-lipids) [62]. BR is a proton-transporting membrane protein, formed of seven transmembrane alpha-helices arranged around the photosensitive retinal molecule. The protein in the lipid matrix is organized in trimers that form a highly ordered 2D hexagonal lattice with lattice parameter $a \sim 62\,\text{Å}$, as depicted in Fig. 10.2b. The structure of PM is well established by electron microscopy, neutron, and X-ray diffraction experiments as reviewed for instance in [62–67].

The dynamic neutron scattering experiments were performed on the IN12 cold triple-axis spectrometer at the ILL. IN12 turned out to be highly suited for elastic and inelastic investigations in oriented biological samples because of its flexibility, good energy resolution, and extremely low background. It allows the measurement of diffraction and inelastic scattering in the same run without changing the set-up, which is crucial to assign dynamical modes to structural properties and molecular components. IN12 was equipped with a vacuum box to avoid air scattering at small scattering angles and with vertically focusing monochromator and analyzer to increase the neutron flux at the sample position. All scans were done with fixed $k_\text{f} = 1.25\,\text{Å}^{-1}$ resulting in a Q resolution of $\Delta Q = 0.005\,\text{Å}^{-1}$ and an energy resolution of $\Delta\hbar\omega = 25\,\mu\text{eV}$.

Deuterated PM was produced and hydrated by H_2O in order to suppress the contribution of the membrane hydration water to the phonon spectrum in the coherent inelastic neutron scattering experiments. Correlations and motions in membranes are often well separated in reciprocal space because of the largely different length and time scales involved. The prominent distances in PM, such as lipid–lipid distances, BR-BR monomer, and trimer distances, lead to correlation peaks. Because the length scales involved span a wide range from 4.5 Å for the lipid chain distance to 62 Å for the trimer-trimer distance, the corresponding signals appear well separated in reciprocal space. The same holds for the different time scales involved from the picoseconds (molecular reorientations) to the nano- or microsecond (membrane undulations, large protein motions). The use of oriented samples further allows separating correlations in the plane of the membranes, and perpendicular to the bilayers. Figure 10.8a depicts energy scans at constant-$q_{||}$ scans at selected values between $q_{||} = 0.35\,\text{Å}^{-1}$ and $q_{||} = 0.45\,\text{Å}^{1}$. The total inelastic signal consists of a Gaussian central peak due to instrumental resolution, a quasielastic broadening, which is described by a Lorentzian peak shape, and pairs of excitations, described by damped harmonic-oscillator peak profiles.

The excitation spectrum of the 2D protein lattice was modeled analytically for comparison with the experimental data. The protein trimers were taken as the centers of a primitive hexagonal lattice with lattice constant $a = 62\,\text{Å}$, and the spectrum of the acoustic phonons was calculated. The model is depicted in Fig. 10.2b. The basic hexagonal translations are marked by arrows. The interaction between the protein trimers is contained in springs with an effective (longitudinal) spring constant k (Fig. 10.2b). The calculated longitudinal spectrum $C_\text{l}(q_{||}, \omega)$, defined by $C_\text{l}(q_{||}, \omega) = (\omega^2/q_{||}^2)S(q_{||}, \omega)$, is shown in Fig. 10.8b. The statistical average in

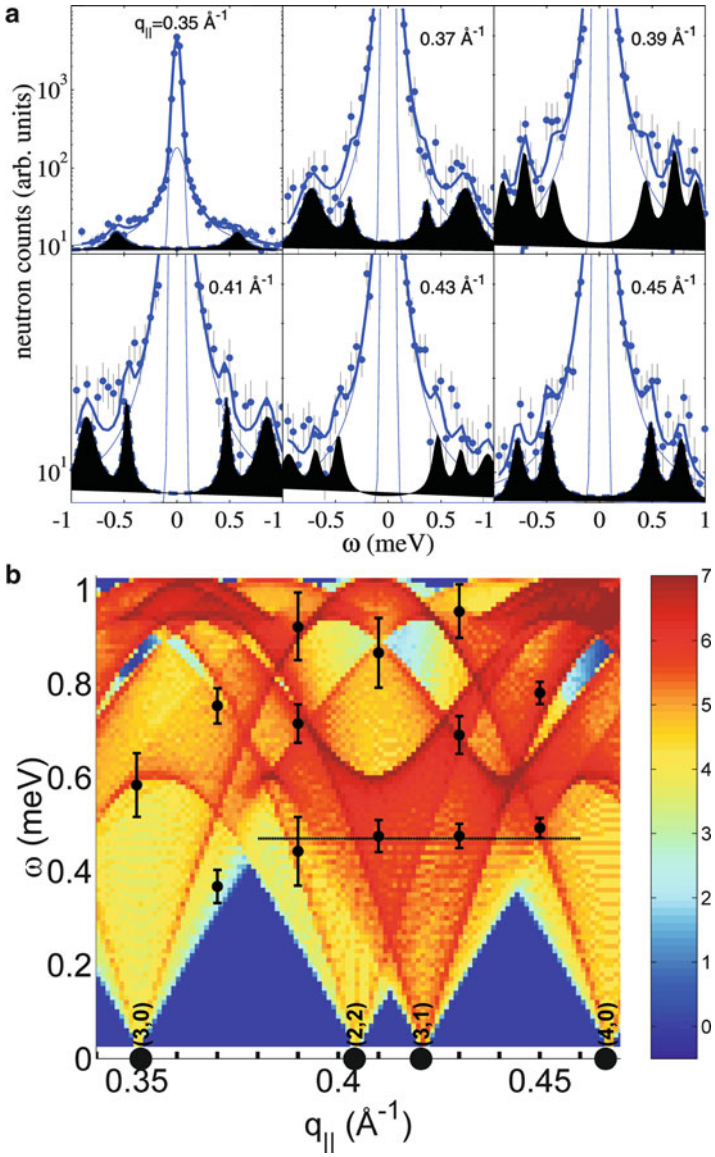

Fig. 10.8 (**a**) Energy scans at $q_{||}$ values of $q_{||} = 0.35$, 0.37, 0.39, 0.41, 0.43, and 0.45 Å^{-1}. The total inelastic signal consists of a central peak (Gaussian), a Lorentzian quasielastic contribution, and the excitations, fitted using damped harmonic-oscillator peak profiles. (**b**) Calculated excitation spectrum $C_l(q_{||}, \omega)$ in the range of the experimental data. Data points mark the positions of excitations, as determined from the fits in part (**a**). The *errorbars* give the uncertainty in determining the peak position. The horizontal line at $\hbar\omega = 0.45$ meV marks the position of a possible optical phonon mode, not included in the calculations (from ref. [68])

the plane of the membrane leads to a superposition of the different phonon branches, which start and end in the hexagonal Bragg peaks (at $\hbar\omega = 0$). The positions of excitations, as determined from the fits in Fig. 10.8a, are marked by the data points. The absolute phonon energies cannot be determined from the model, but depend on the coupling constant k. So the energy of the phonon spectrum in Fig. 10.8b was fitted to best match the experiment. The experimentally determined excitation energies occur at the intersections of the inelastic scans with the calculated phonon branches and well reproduce the features of the theoretical excitation spectrum within the given errors. Note that because the proteins trimers were treated as dots with an effective mass of M_{tr}, the calculations do not include any contributions from intramonomer or intratrimer dynamics, i.e., possible optical modes. The excitations observed in the experiment at $q_{||}$ values around $0.42\,\text{Å}^{-1}$ (corresponding to a length scale of about 15 Å) and energy value of 0.45 meV (marked by the solid line in Fig. 10.8b) have no equivalent in the theoretical spectrum and possibly stem from optical phonon branches. Because the distance agrees well with the monomer–monomer distance in the protein trimer, this mode can tentatively be assigned to optical-like monomer dynamics (the corresponding form factor is likely to be maximum at the corresponding nearest neighbor distance).

The commonly assumed interaction mechanism between inclusions in membranes is a lipid-mediated interaction due to local distortions of the lipid bilayer [20–24], with a strong dependence on the bilayer properties, in particular elastic properties. The PM may, however, be a special case because there are very few lipids between neighboring BR proteins [69]. While the nature of the interaction still will be mainly elastic, it is not likely to be purely lipid-mediated but partially a direct protein–protein interaction. The strength of the interaction can be determined from the data in Fig. 10.8. The energy of the zone-boundary phonon at the M-point of the hexagonal Brillouin zone (for instance, at a $q_{||}$ value of $0.35\,\text{Å}^{-1}$) relates to the coupling constant by $M_{\mathrm{tr}}\omega^2 = 6k$. Because the energy is determined to $\hbar\omega = 1.02\,\text{meV}$, the effective protein–protein spring constant k is calculated to about $k = 54\,\text{N m}^{-1}$. The amplitude of this mode of vibration can be estimated from the equipartition theorem to $\sqrt{\langle x^2\rangle} = \sqrt{k_{\mathrm{B}}T/k} = 0.1\,\text{Å}$, and the interaction force between two neighboring trimers to $F = k\sqrt{\langle x^2\rangle} = 0.5\,\text{nN}$. Using the same approach, the spring constant for graphite for comparison is calculated to $27{,}000\,\text{N m}^{-1}$ for the in-plane interaction, and $3.5\,\text{N m}^{-1}$ for out-of-plane interactions. The force constant that we measure in PM is 1–2 orders of magnitude larger than the effective van-der-Waals force constant in graphite, but 2–3 orders of magnitude weaker than a C–C bond.

The mechanism reported here may be relevant to model the photo cycle in PM. It was reported [70] that the BR proteins undergo structural changes during the photo cycle, involving displacements of up to 1.7 Å. Because of the elastic coupling of the BR proteins, those displacements can propagate to neighboring proteins. On the microscopic level, displacing or distorting a BR trimer by 1.7 Å yields a force between neighboring trimers of 9 nN (using the model presented here). It can therefore be speculated that there is a protein–protein communication during the photocycle in PM.

10.4.4 Single Particle vs Collective Dynamics

The "softness" of the BR proteins in PM was also probed by elastic incoherent neutron scattering [71], and force constants of $0.1\,\mathrm{N\,m^{-1}}$ were reported. The shear modulus in stacks of PM was determined by X-ray reflectivity to $\mu = 0.02\,\mathrm{N\,m^{-1}}$ [65]. The corresponding amplitudes of vibration were 2.2 Å, respective 3.8 Å. These techniques were mainly sensitive to diffusion of proteins (and lipids), and the force and time constants involved are determined by local friction and restoring forces. The corresponding force constants are about two orders of magnitude smaller than the one reported here. Energies of collective, phonon-like excitations were also reported for proteins in a protein crystal (from computer simulations in refs. [8, 72]) and hydrated protein powder (from inelastic X-ray scattering [73]), and energies of about 1 meV for inter- and even 10 meV for intraprotein motions were found. The reported energies cannot be quantitatively compared to the excitations in this study because the systems are distinctly different. However, it seems that the energies found for protein interactions are consistently higher than the force constants from experiments, which probe the local energy landscapes. The amplitudes of diffusive, self-correlated motions are therefore about one magnitude larger than those of collective, pair-correlated motions. "Motional coherence," i.e., a structurally coherent state, was reported recently in fluid phospholipid membranes [74]. The authors reported that lipids move as coherently coupled clusters of about 30 Å rather than individual lipids. As a consequence, micrometer lipid diffusion may appear slow when studied with mesoscopic techniques such as fluorescent light microscopy because the movement of clusters is measured rather than the motion of individual lipids. Diffusion constants from incoherent neutron scattering are usually faster because they measure fast motions of lipids over much shorter, nanometer distances. So while for a long time, motions in biological materials were considered as thermally activated vibrations or librations in local potentials, at least part of the fluctuation spectrum stems from interactions. The future challenge is to understand the impact of collective molecular motions in membranes and proteins on biological function.

Acknowledgments It is my pleasure to thank all my colleagues who were involved in the original work and publications. The data presented here were collected at the high flux reactor of the Institut Laue-Langevin in Grenoble

References

1. Rheinstädter MC, Seydel T, Häußler W, Salditt T (2006) Exploring the collective dynamics of lipid membranes with inelastic neutron scattering. J Vac Sci Technol A 24:1191–1196
2. Voïtchovsky K, Contera SA, Ryan JF (2009) Lateral coupling and cooperative dynamics in the function of the native membrane protein bacteriorhodopsin. Soft Mat 5:4899

3. Frauenfelder H, Sligar S, Wolynes P (1991) The energy landscapes and motions of proteins. Science 254:1598–1603
4. Fenimore P, Frauenfelder H, McMahon B, Young R (2004) Bulk-solvent and hydration-shell fluctuations, similar to α- and β-fluctuations in glasses, control protein motions and functions. Proc Natl Acad Sci U S A 101:14408–14413
5. Bayerl T (2000) Collective membrane motions. Curr Opin Colloid Interface Sci 5:232–236
6. Rheinstädter MC, Häussler W, Salditt T (2006) Dispersion relation of lipid membrane shape fluctuations by neutron spin-echo spectrometry. Phys Rev Lett 97:048103
7. Smith JC (1991) Protein dynamics: comparison of simulations with inelastic neutron scattering experiments. Q Rev Biophys 24:227–291
8. Hayward JA, Smith JC (2002) Temperature dependence of protein dynamics: computer simulation analysis of neutron scattering properties. Biophys J 82:1216–1225
9. Tarek M, Tobias D, Chen S-H, Klein M (2001) Short wavelength collective dynamics in phospholipid bilayers: a molecular dynamics study. Phys Rev Lett 87:238101
10. Tarek M, Tobias D (2002) Role of protein-water hydrogen bond dynamics in the protein dynamical transition. Phys Rev Lett 88:138101
11. Wood K, Plazanet M, Gabel F, Kessler B, Oesterhelt D, Tobias DJ, Zaccai G, Weik M (2007) Coupling of protein and hydration-water dynamics in biological membranes. Proc Natl Acad Sci U S A 104:18049–18054
12. Meinhold L, Smith JC, Kitao A, Zewail AH (2007) Picosecond fluctuating protein energy landscape mapped by pressure—temperature molecular dynamics simulation. Proc Natl Acad Sci U S A 104:17261–17265
13. Salditt T (2000) Structure and fluctuations of highly oriented phospholipid membranes. Curr Opin Colloid Interface Sci 5:19–26
14. Krueger S (2001) Neutron reflection from interfaces with biological and biomimetic materials. Curr Opin Colloid Interface Sci 6:111–117
15. Salditt T (2005) Thermal fluctuations and stability of solid-supported lipid membranes. J Phys Condens Matter 17:R287–R314
16. Kučerka N, Nieha M-P, Pencera J, Harroun T, Katsaras J (2007) The study of liposomes, lamellae and membranes using neutrons and X-rays. Curr Opin Colloid Interface Sci 12:17–22
17. Krueger S, Meuse C, Majkrzak C, Dura A, Berk NF, Tarek M, Plant AL (2001) Investigation of hybrid bilayer membranes with neutron reflectometry: probing the interactions of melittin. Langmuir 17:511–521
18. Fragneto G, Rheinstädter M (2007) Structural and dynamical studies from bio-mimetic systems: an overview. C R Phys 8:865–883
19. Tanaka M, Sackmann E (2005) Polymer-supported membranes as models of the cell surface. Nature 437:656–663
20. Kralchevsky PA (1997) Lateral forces acting between particles in liquid films or lipid membranes. Adv Biophys 34:25–39
21. Bohinc K, Kralj-Iglic V, May S (2003) Interaction between two cylindrical inclusions in a symmetric lipid bilayer. J Chem Phys 119:7435–7444
22. Biscari P, Bisi F (2002) Membrane-mediated interactions of rod-like inclusions. Eur Phys J E 6:381–386
23. Lagüe P, Zuckermann MJ, Roux B (2001) Lipid-mediated interactions between intrinsic membrane proteins: dependence on protein size and lipid composition. Biophys J 81:276–284
24. Dan N, Pincus P, Safran S (1993) Membrane-induced interactions between inclusions. Langmuir 9:2768–2771
25. König S, Pfeiffer W, Bayerl T, Richter D, Sackmann E (1992) Molecular dynamics of lipid bilayers studied by incoherent quasi-elastic neutron scattering. J Phys II (France) 2:1589–1615
26. König S, Sackmann E, Richter D, Zorn R, Carlile C, Bayerl T (1994) Molecular dynamics of water in oriented DPPC multilayers studied by quasielastic neutron scattering and deuterium-nuclear magnetic resonance relaxation. J Chem Phys 100:3307–3316
27. König S, Bayerl T, Coddens G, Richter D, Sackmann E (1995) Hydration dependence of chain dynamics and local diffusion in L-alpha-dipalmitoylphosphatidylcholine multilayers studied by incoherent quasi-elastic neutron scattering. Biophys J 68:1871–1880

28. Pfeiffer W, Henkel T, Sackmann E, Knorr W (1989) Local dynamics of lipid bilayers studied by incoherent quasi-elastic neutron scattering. Europhys Lett 8:201–206
29. Pfeiffer W, König S, Legrand J, Bayerl T, Richter D, Sackmann E (1993) Neutron spin echo study of membrane undulations in lipid multibilayers. Europhys Lett 23:457–462
30. Lindahl E, Edholm O (2000) Mesoscopic undulations and thickness fluctuations in lipid bilayers from molecular dynamics simulations. Biophys J 79:426–433
31. Lipowsky R, Sackmann E (eds) (1995) Structure and dynamics of membranes. Elsevier, Amsterdam
32. Nevzorov A, Brown M (1997) Bilayers from comparative analysis of 2H and 13C NMR relaxation data as a function of frequency and temperature. J Chem Phys 107:10288–10310
33. Bloom M, Bayerl T (1995) Membranes studied using neutron scattering and NMR. Can J Phys 73:687–696
34. Takeda T, Kawabata Y, Seto H, Komura S, Gosh S, Nagao M, Okuhara D (1999) Neutron spin echo investigations of membrane undulations in complex fluids involving amphiphiles. J Phys Chem Solids 60:1375–1377
35. Hirn R, Bayerl T, Rädler J, Sackmann E (1999) Collective membrane motions of high and low amplitude, studied by dynamic light scattering and micro-interferometry. Faraday Discuss 111:17–30
36. Hirn RB, Bayerl TM (1999) Collective membrane motions in the mesoscopic range and their modulation by the binding of a monomolecular protein layer of streptavidin studied by dynamic light scattering. Phys Rev E 59:5987–5994
37. Hildenbrand MF, Bayerl TM (2005) Differences in the modulation of collective membrane motions by ergosterol, lanosterol, and cholesterol: a dynamic light scattering study. Biophys J 88:3360–3367
38. Squires G (1978) Introduction to the theory of thermal neutron scattering. Dover, New York
39. Lovesey S (1984) Theory of neutron scattering from condensed matter. Clarendon Press, Oxford
40. Liao C, Chen S, Sette F (2000) Analysis of inelastic X-ray scattering spectra of low-temperature water. Phys Rev E 61:1518–1526
41. Chen S, Liao C, Huang H, Weiss T, Bellisent-Funel M, Sette F (2001) Collective dynamics in fully hydrated phospholipid bilayers studied by inelastic X-ray scattering. Phys Rev Lett 86:740–743
42. Rheinstädter MC, Ollinger C, Fragneto G, Demmel F, Salditt T (2004) Collective dynamics of lipid membranes studied by inelastic neutron scattering. Phys Rev Lett 93:108107
43. Mezei F (ed) (1980) Neutron spin echo. Springer, Heidelberg
44. Chu N, Kučerka N, Liu Y, Tristram-Nagle S, Nagle JF (2005) Anomalous swelling of lipid bilayer stacks is caused by softening of the bending modulus. Phys Rev E 71:041904
45. Jenskea R, Lindström F, Gröbner G, Vettera W (2008) Impact of free hydroxylated and methyl-branched fatty acids on the organization of lipid membranes. Chem Phys Lipids 154:26–32
46. Aussenac F, Laguerre M, Schmitter J-M, Dufourc EJ (2003) Detailed structure and dynamics of bicelle phospholipids using selectively deuterated and perdeuterated labels. ^{2}H NMR and molecular mechanics study. Langmuir 19:10468–10479
47. Rheinstädter MC, Seydel T, Salditt T (2007) Nanosecond molecular relaxations in lipid bilayers studied by high energy resolution neutron scattering and in-situ diffraction. Phys Rev E 75:011907
48. Hub JS, Salditt T, Rheinstädter MC, de Groot BL (2007) Short range order and collective dynamics of DMPC bilayers. A comparison between molecular dynamics simulations, X-ray, and neutron scattering experiments. Biophys J 93:3156–3168. doi:dx.doi.org
49. Kučerka N, Liu Y, Chu N, Petrache HI, Tristram-Nagle S, Nagle JF (2005) Structure of fully hydrated fluid phase DMPC and DLPC lipid bilayers using X-ray scattering from oriented multilamellar arrays and from unilamellar vesicles. Biophys J 88:2626–2637
50. de Schepper I, Verkerk P, van Well A, de Graaf L (1983) Short-wavelength sound modes in liquid argon. Phys Rev Lett 50:974–977

51. van Well A, Verkerk P, de Graaf L, Suck J-B, Copley J (1985) Density fluctuations in liquid argon: coherent dynamic structure factor along the 120-K isotherm obtained by neutron scattering. Phys Rev A 31:3391–3414
52. van Well A, de Graaf L (1985) Density fluctuations in liquid neon studied by neutron scattering. Phys Rev A 32:2396–2412
53. Glyde H (1994) Excitations in liquid and solid helium. Clarendon Press, Oxford
54. Caillé A (1972) X-ray scattering by smectic-A crystals. C R Acad Sci Ser B 274:891–893
55. Lei N, Safinya C, Bruinsma R (1995) Discrete harmonic model for stacked membranes: theory and experiment. J Phys II 5:1155–1163
56. Lyatskaya Y, Liu Y, Tristram-Nagle S, Katsaras J, Nagle JF (2000) Method for obtaining structure and interactions from oriented lipid bilayers. Phys Rev E 63:011907
57. Salditt T, Vogel M, Fenzl W (2003) Thermal fluctuations and positional correlations in oriented lipid membranes. Phys Rev Lett 90:178101
58. Romanov V, Ul'yanov S (2002) Dynamic and correlation properties of solid supported smectic-A films. Phys Rev E 66:061701
59. Bary-Soroker H, Diamant H (2007) Nanoscale surface relaxation of a membrane stack. Phys Rev E 76:042401
60. Bary-Soroker H, Diamant H (2006) Surface relaxation of lyotropic lamellar phases. Europhys Lett 73:871–877
61. Ribotta R, Salin D, Durand G (1974) Quasielastic rayleigh scattering in a smectic-A crystal. Phys Rev Lett 32:6–9
62. Haupts U, Tittor J, Oesterhelt D (1999) Closing in on bacteriorhodopsin: progress in understanding the molecule. Annu Rev Biophys Biomol Struct 28:367–399
63. Zaccai G (2000) Moist and soft, dry and stiff: a review of neutron experiments on hydration-dynamics-activity relations in the purple membrane of Halobacterium salinarum. Biophys Chem 86:249–257
64. Koltover I, Salditt T, Rigaud J-L, Safinya C (1998) Stacked 2D crystalline sheets of the membrane-protein bacteriorhodopsin: a specular and diffuse reflectivity study. Phys Rev Lett 81:2494–2497
65. Koltover I, Rädler J, Salditt T, Safinya C (1999) Phase behavior and interactions of the membrane-protein bacteriorhodopsin. Phys Rev Lett 82:3184–3187
66. Neutze R, Pebay-Peyroula E, Edman K, Royant A, Navarro J, Landau E (2002) Bacteriorhodopsin: a high resolution structural view of vectorial proton transport. Biochim Biophys Acta 1565:144–167
67. Lanyi J (2004) Bacteriorhodopsin. Annu Rev Physiol 66:665–688
68. Rheinstädter MC, Schmalzl K, Wood K, Strauch D (2009) Protein-protein interaction in purple membrane. Phys Rev Lett 103:128104
69. Baudry J, Tajkhorshid E, Molnar F, Phillips J, Schulten K (2001) Molecular dynamics study of bacteriorhodopsin and the purple membrane. J Phys Chem 105:905–918
70. Luecke H, Schobert B, Richter H-T, Cartailler J-P, Lanyi JK (1999) Structural changes in bacteriorhodopsin during ion transport at 2 angstrom resolution. Science 286:255–260
71. Zaccai G (2000) How soft is a protein? A protein dynamics force constant measured by neutron scattering. Science 288:1604–1607
72. Kurkal-Siebert V, Agarwal R, Smith JC (2008) Hydration-dependent dynamical transition in protein: protein interactions at ≈240 K. Phys Rev Lett 100:138102
73. Liu D, Chu X-Q, Lagi M, Zhang Y, Fratini E, Baglioni P, Alatas A, Said A, Alp E, Chen S-H (2008) Studies of phononlike low-energy excitations of protein molecules by inelastic X-ray scattering. Phys Rev Lett 101:135501
74. Rheinstädter MC, Das J, Flenner EJ, Brüning B, Seydel T, Kosztin I (2008) Motional coherence in fluid phospholipid membranes. Phys Rev Lett 101:248106